Max-Planck-Institut
für Quantenoptik
SIBLIOTHEK
D-8046 Garching

MAX-PLANCK-INSTITUT FÜR QUANTENOPTIK

ICF-Target Studies for Heavy Ion Fusion

J. Meyer-ter-Vehn

M P Q 64

July 1982

MPQ-Report
64

Dieser MPQ-Bericht ist als Manuskript des Autors gedruckt
Alle Rechte vorbehalten

This MPQ-report has been printed as author's manuscript
All rights reserved

MAX-PLANCK-INSTITUT FÜR QUANTENOPTIK

ICF-Target Studies for Heavy Ion Fusion

J. Meyer-ter-Vehn

Max-Planck-Institut
für Quantenoptik
BIBLIOTHEK
D-8046 Garching

M P Q 64 July 1982

MPQ 64

ICF-Target Studies for Heavy Ion Fusion

J. Meyer-ter-Vehn

Invited Talk
at the Symposium on Accelerator Aspects of Heavy Ion Fusion at
Gesellschaft für Schwerionenforschung Darmstadt, West Germany
March 29 - April 2, 1982

In this talk, work on ICF targets for Heavy Ion Fusion (HIF) performed at the Max-Planck-Institut for Quantum Optics (MPQ) at Garching in the period 1979-1982 is presented[1]. It is part of the German feasibility study of inertial confinement fusion (ICF) by means of heavy ion beams[2,3]. Within this project target aspects are also studied at the Kernforschungszentrum Karlsruhe with emphasis on thermonuclear burn and transport in a reactor cavity and at the universities in Frankfurt and Darmstadt with focus on symmetry aspects and more-dimensional simulation. The work at MPQ has been performed by Dr. Metzler, Dipl. Math. Schalk, Dipl. Math. Lackner (since October 1981) and myself.

Target performance is a key issue for inertial confinement fusion. Thermonuclear burn of a few mg DT fuel has to be achieved in the highly compressed target core after beam driven implosion. A central quantity is the target gain

$$G = E_{TN}/E_{Beam}$$

This work was supported by the Bundesministerium für Forschung und Technologie (Contract 06 SIT 28)

which is the ratio of thermonuclear energy output E_{TN} to beam energy input E_{Beam}. The gain depends on beam parameters such as

ion species (mass A_{ion}, charge Z_{ion})
ion energy E_{ion}
maximum beam current I_{Beam}
focal spot size
temporal pulse shape
number of beams and irradiation symmetry

and target parameters such as

target structure (geometry, layers, materials)
target size and mass

and a number of other parameters. A major objective of our work has been to understand the basic relations between these parameters and to identify the most critical points.

Fuel ignition, i.e. DT-burn selfsustained by α particle heating, is necessary to obtain a target gain larger than one. High gain in the order of 100 as needed for a power reactor requires DT-burn propagating from the ignited region into a reservoir of non-ignited DT-fuel. Spherical symmetry during target implosion turns out to be a most critical point in this context. Spherical convergence considerably helps to achieve the high concentration of specific energy $\varepsilon_{ign} \cong 600$ MJ/g in the center which is needed for DT ignition. In order to assure a sufficient degree of implosion symmetry, one has either to care for a very uniform irradiation of the target (directly driven targets) or to smooth beam asymmetries in the target, e.g. by first converting beam energy into thermal radiation which fills a target cavity isotropically and drives an inner target (radiatively driven targets, see energy conversion scheme)[4]. Our work presented below is concentrated on the direct drive approach, but it should be clear that the symmetry question is crucial and radiative smoothing

Scheme 1. Beam energy conversion in directly driven targets (left side) and radiatively driven targets (right side)

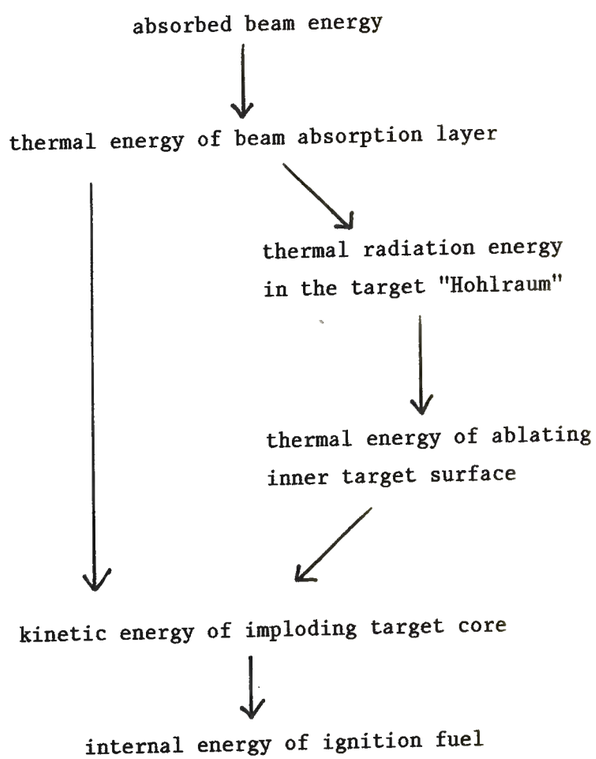

Only a small fraction η (hydrodynamic efficiency) of the absorbed beam energy is converted into fuel energy at ignition.

---

may be a superior solution. The physics of ion energy deposition in high-Z solid material offer itself for x-ray conversion. The flux of black body radiation from a heated surface is $S \cong 10^{13}$ W/cm^2 (T[100 eV])^4 and is equal to the required beam power of some 100 TW/cm^2 at a temperature of 200 - 300 eV which is typically reached in the absorbing layer of HIF targets as discussed below.

The individual topics to be touched in the following are:

1. Model for ICF target gain
2. Scaling relations for directly driven HIF targets
3. Heavy ion stopping calculations
4. 1D target calculations for HIBALL

   4.1 General picture of a HIF target implosion
   4.2 Optimal ion energy and tamper/absorber ratio
   4.3 The ignition problem

5. Selfsimilar compression waves
6. Foil irradiation with a cylindrical heavy ion beam. Scaling and simulation with 2D PIC code.
7. Conclusions.

1. Model for ICF target gain[5)]

We have considerably improved a model for energy gain of ICF targets which had been formulated before by R. Kidder[6)] and S. Bodner[7)]. The model allows to reproduce Livermore gain predictions[8)] in terms of a few key parameters and to specify the parameter region relevant for power reactors. A most essential parameter is the size of the igniting fuel region (spark radius) which is intimately related to the degree of implosion symmetry.

The underlying model assumes a DT fuel configuration at ignition as shown in Fig. 1. It consists of a central hot region (spark) surrounded by highly compressed fuel at low entropy. We have modified the model by assuming uniform pressure over the fuel region at ignition instead of uniform density. This is suggested by code calculations as well as self-similar implosions and leads to substantially improved results. The free model parameters are:

(1) the hydrodynamic efficiency η which is the fraction of beam energy transfered into internal energy of the fuel at ignition ($E_{Fuel} = \eta E$ ... see scheme 1)

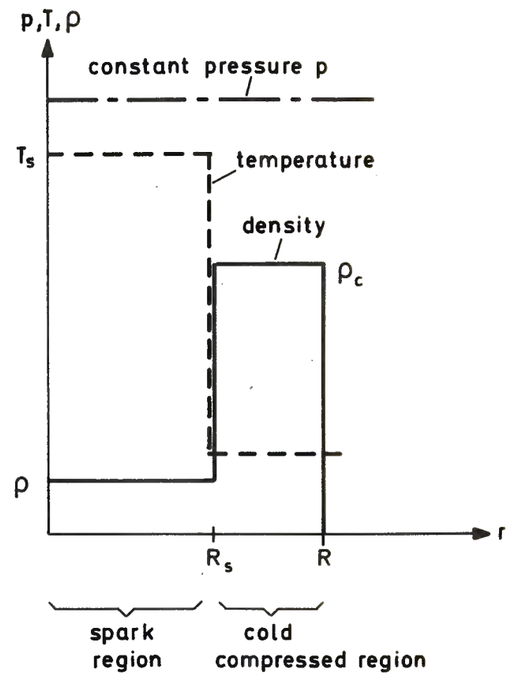

Fig. 1: Profiles for pressure, temperature and density of the model ignition configuration.

(2) the isentrope parameter α which gives the pressure of the highly compressed fuel region in units of the electron degeneracy pressure ($p = \alpha p_{deg}$) and describes the degree of adiabaticity during implosion, and

(3) the spark radius R_S which is constrained by deviations from spherical implosion symmetry and is therefore a most significant parameter for target performance.

Further parameters fixed by DT fusion physics are the ignition temperature $kT_S \cong 5$ keV, the spark $\rho_S R_S \cong 0.4$ g/cm^2 roughly equal to the α particle range, and the fraction of burned fuel $\Phi = H_F/(H_B + H_F)$ where $H_F = (\rho R)_{Fuel}$ is the total fuel ρR and $H_B \cong 7$ g/cm^2. These rather general parameters with clear physical significance are sufficient to calculate the gain within the model. Details are given in Ref. 5.

In Fig. 2, the Livermore gain predictions for reactor targets based on extensive code calculations are compared with the present model. They are

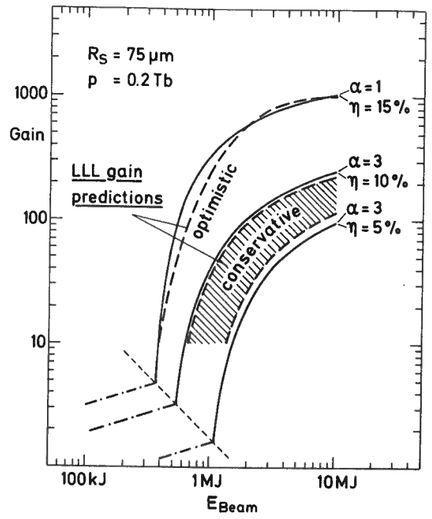

Fig. 2: Fit of the present model to Livermore gain predictions for reactor targets. The thin broken line marks the ignition threshold.

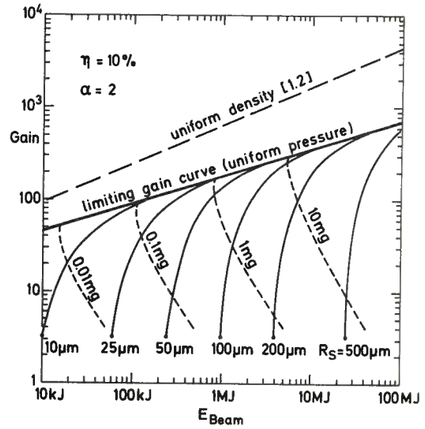

Fig. 3: Gain curves for fixed isentrope α and hydroefficiency η and increasing spark radius R_S. Lines of equal fuel mass M_F (short dashes) are labeled by the mass value. Limiting gain curves are shown for the present model assuming uniform pressure as well as for the Kidder-Bodner model assuming uniform density.

well reproduced with a spark radius of $R_S \cong 75$ µm or, equivalently, a spark pressure of p = 0.2 Tbar. The 'conservative gain band' corresponds to an hydrodynamic efficiency ranging between 5 % < η < 10 % and to a cold fuel isentrope α = 3. This may be called conservative in comparison with the 'optimistic gain curve' which is obtained with α = 1 and η = 15 % and is close to the physical limits.

Figure 3 displays the decisive role of the spark radius R_S for expected gain and ignition energy. It is predominantly the limits on R_S which drive up the requirements on beam energy. Hydrodynamic efficiency and

isentrope have been fixed at η = 10 % and α = 2. Gain 60 could be reached with E_{Beam} = 100 kJ provided it would be possible to make a 10 µm spark at this low preheat level. In case of ion beam targets where beam focusing is a problem and rather large targets (R_o > 1 mm) have to be used this option is unrealistic - at least for directly driven targets - because of a convergence ratio R_S/R_o less than 1 %. The expected option for high-gain reactor targets is located in Fig. 3 in the region

$$G \cong 100$$
$$1\ MJ < E_{Beam} < 10\ MJ$$
$$50\ \mu m < R_{Spark} < 200\ \mu m$$
$$1\ mg < M_{Fuel} < 10\ mg$$

The upper limit is given by the requirement of containing the micro-explosion in the reactor.

An interesting feature of the gain model is that there exists a limiting gain curve which determines the maximum gain possible at a given level of beam energy for any spark radius. In fact, G as a function of R_S at fixed E_{Beam} and all other parameters fixed has a maximum G* which defines the limiting gain curve and appears in Fig. 3 as the envelope of the individual gain curves with different R_S. The broken line in Fig. 3 represents the limiting gain curve under the assumption of uniform density of the fuel at ignition (model of Kidder and Bodner). This leads to considerably more optimistic gain which is, however, not realistic.

2. Scaling relation for directly driven HIF targets

Estimates for the beam power

$$P_{Beam} = E_{ion} \cdot I_{Beam} \qquad (1)$$

and the particle beam current I_{Beam} which are required for target ignition have been obtained from a simple model consideration involving

the ion energy E_{ion}
the ion range $R(E_{ion})$
the beam pulse time t_{pulse}
the beam focus radius r_{focus}

A directly driven target is assumed as shown in Fig. 4. It consists of a hollow sphere with an absorbing layer of density ρ and thickness d and a thin fuel layer at the inner surface of the sphere with a radius

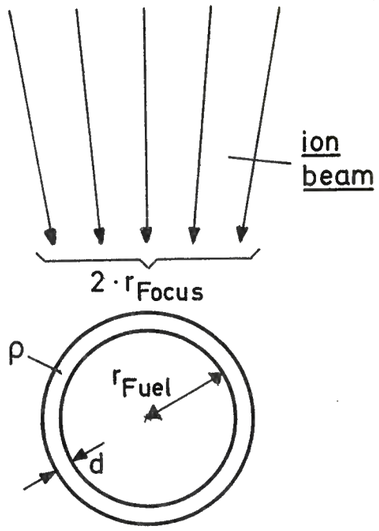

Fig. 4: HIF target schematically. Only one of the beams irradiating the target is shown.

r_{fuel}. One wants to have the target size as small as possible in order to minimize the requirements on beam power and energy. On the other hand, one has to catch the beam. It is therefore assumed

$$d \ll r_{fuel} \cong r_{focus} \qquad (2)$$

The specific energy deposition in the target is then given by

$$\varepsilon \cong \frac{E_{Beam}}{\text{Absorber Mass}} \cong \frac{E_{ion} \cdot I_{Beam} \cdot t_{pulse}}{4\pi\, r_{fuel} \cdot d \cdot \rho}$$

The pulse time is related to the implosion velocity

$$u_{impl} \cong r_{fuel}/t_{pulse}$$

and this leads with $R \cong \rho d$ to the scaling relation

$$\varepsilon \cong \frac{1}{4\pi\, u_{impl}} \cdot \frac{E_{ion}}{R(E_{ion})} \cdot \frac{I_{Beam}}{r_{focus}} \qquad (3)$$

which factorizes into a target factor, a beam stopping factor and a 'beam brightness' factor. The specific energy deposition needed to ignite DT fuel is known from implosion calculations to be in the region of

$$\varepsilon \cong 20 - 40 \text{ MJ/g} \qquad (4)$$

corresponding to implosion velocities

$$u_{impl} \cong \sqrt{2\varepsilon} \cong (2\text{-}3) \cdot 10^7 \text{ cm/sec} \qquad (5)$$

With these values, the specific energy concentration of 600 MJ/g needed for ignition can be achieved by spherical convergence effects in the implosion center. From eqs. (1) - (5) one obtains for the required beam power

$$P_{Beam} \cong 2\pi(2\varepsilon)^{3/2} \cdot R(E_{ion}) \cdot r_{focus} \qquad (6)$$

which shows the importance of small ion range and a small focal radius which sets a lower bound on the target radius. Taking HIBALL values

$$
\begin{aligned}
r_{focus} &= 3 \text{ mm} \\
E_{ion} &= 10 \text{ GeV} \\
R(E_{ion}) &= 0.3 \text{ g/cm}^2 \quad \text{(Bi-ion on Pb)}
\end{aligned}
\tag{7}
$$

one obtains with $\varepsilon = 20$ MJ/g

$$
\begin{aligned}
P_{Beam} &= 500 \text{ TW} \\
I_{Beam} &= 50 \text{ kA} \\
t_{pulse} &= 15 \text{ nsec} \\
E_{Beam} &= 7.5 \text{ MJ}
\end{aligned}
\tag{8}
$$

These values are typical for a HIF reactor target.

3. Heavy ion stopping calculations

We have calculated ranges and profiles of energy deposition of heavy ions in hot dense plasma using standard stopping theory. Details have been outlined in refs. 1. Some typical results for Bi-ions on Pb and Li (HIBALL absorber materials) are given in Fig. 5 and Fig. 6. In the region of low E_{ion} (some MeV/amu) our theoretical model has been adjusted to recent GSI stopping data[9].

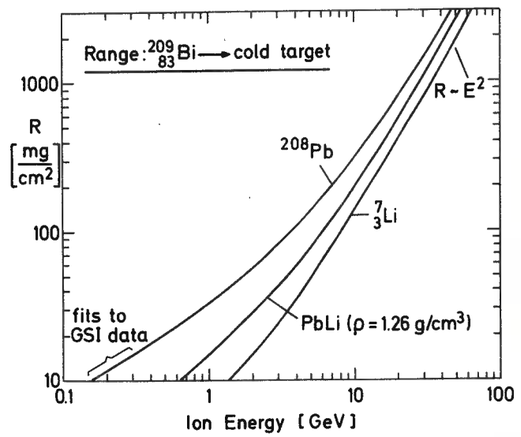

Fig. 5: Calculated ranges of Bi-ions in different solid materials as a function of

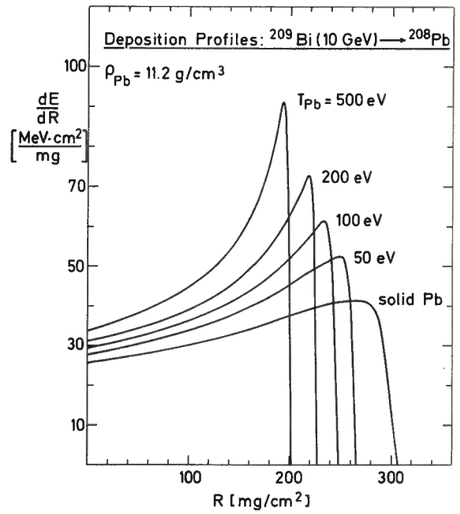

Fig. 6: Calculated stopping power as a function of range for Bi on Pb for different target temperatures.

4. 1D target calculations for HIBALL

In connection with the HIBALL reactor study[3], we have studied heavy ion driven target implosions with the 1D code MINIHY which has been developed by N. Metzler. A description of the code and first results have been published in ref. 1 and in the HIBALL report; a more detailed account on this work is in preparation[10]. It should be clear that there has been no specific experience with respect to ICF target simulation in Germany so far and we had to start from scratch. The results shown in the following provide an overall picture of ion driven implosions, determine optimal ion energy and optimal absorber structure under certain assumptions and deal with the question of pulse shape and ignition in terms of three specific cases. The conclusions should still be considered as preliminary, in particular concerning the last point since radiation transport is not included in the simulation so far.

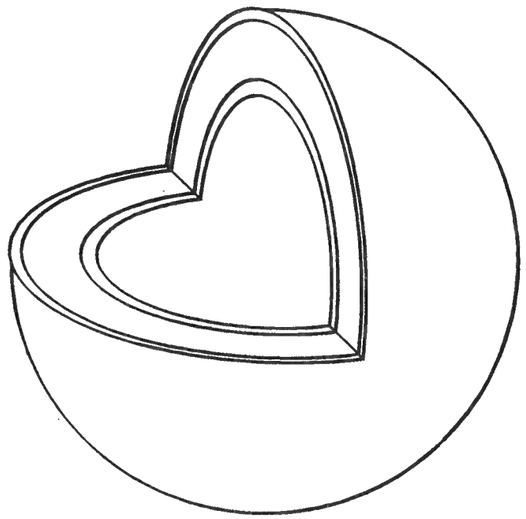

Fig. 7: Perspective view of the HIBALL target

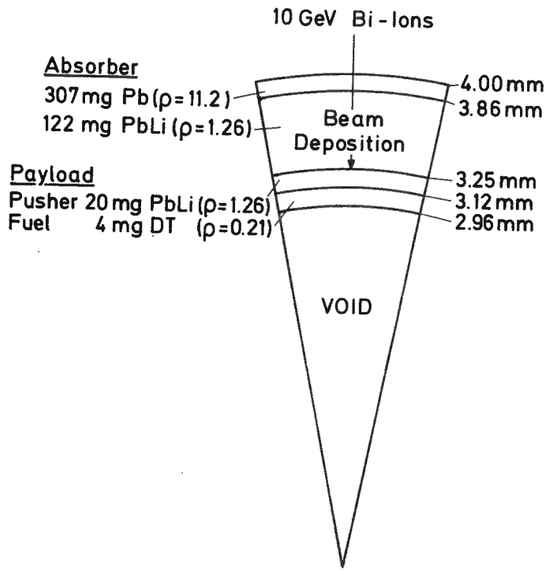

Fig. 8: Sector of the HIBALL target with 4 mg DT fuel

4.1 General picture of a HIF target implosion

A perspective view of the HIBALL target is given in Fig. 7 and a sector cut with materials, masses and initial radii in Fig. 8. It is a single-shell target with three material layers: a Pb tamper outside, a low density PbLi layer in the middle and the DT fuel layer inside. The target radius has been set equal to the expected focal spot radius of the beam. The density and the energy deposition profile of 10 GeV incident Bi-ions at irradiation start time is shown in Fig. 9. Most of the target material is used for beam stopping. Only a small part of the PbLi layer is used as a pusher which separates the fuel from the hot deposition region. The dynamic response of the target to a box shaped pulse with uniform power of 500 TW delivering 5 MJ in 10 nsec is displayed in Fig. 10. The heated absorbing layer (typical temperatures 100-400 eV and pressures around 100 Mbar) is exploding driving the payload (pusher and fuel) at its inner front. Void closure occurs at 18.3 nsec. At 20.4 nsec, the ignition temperature of 5 keV is reached in the center of the fuel (spark),

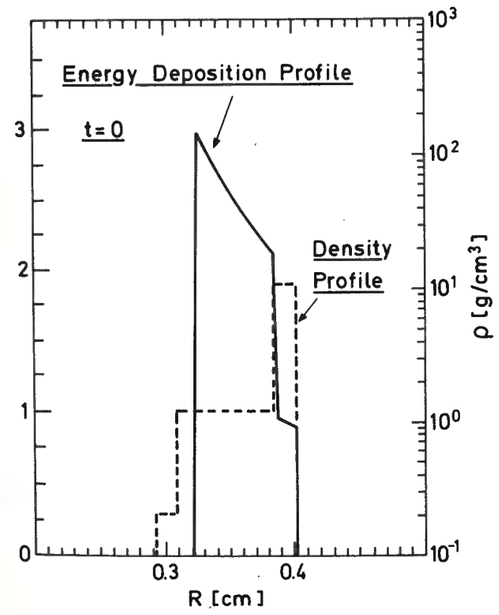

Fig. 9: Initial density and energy deposition profiles

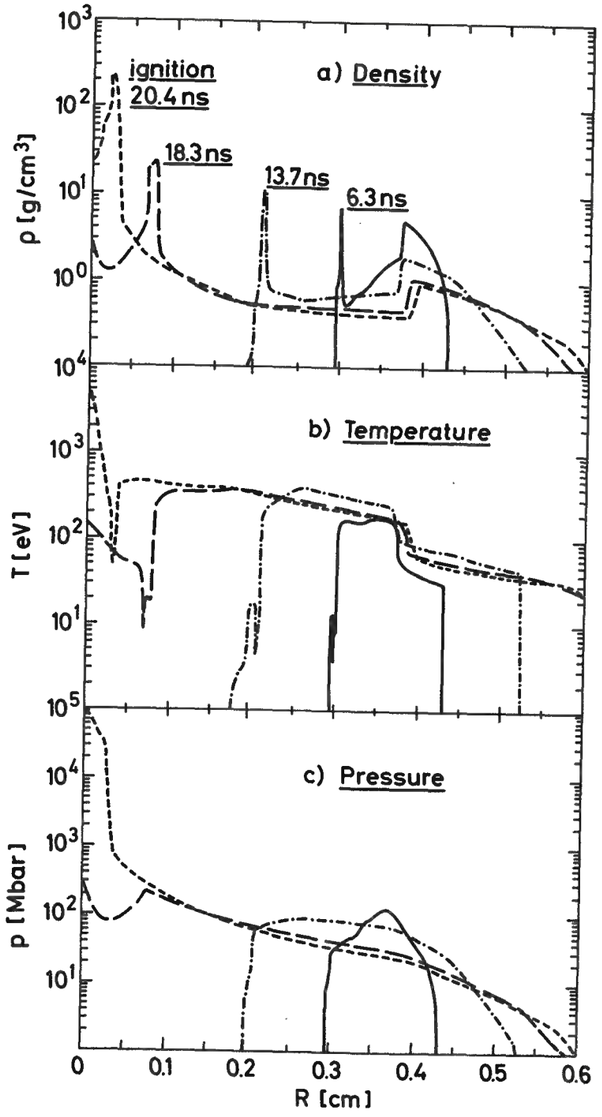

Fig. 10: Evolution of density, temperature and pressure profiles under the action of a box pulse of P_{Beam} = 500 TW, E_{Beam} = 5 MJ and t_{pulse} = 10 nsec.

whereas the outer fuel regions are still at much lower temperature (cold compressed fuel). A strong shock is running outwards at this time as seen in the pressure profile. More details about shock propagation in the fuel and formation of the ignition configuration will be discussed later. First the question of hydrodynamic efficiency and how it depends on ion energy and layer sturcture is investigated.

4.2 Optimal ion energy and tamper/absorber ratio

Hydrodynamic efficiency η is an important parameter for determining the target gain. The question is how to drive a given payload mass in the most efficient way in order to optimize η. Certainly, the ratio between the driving mass of the absorbing layers and the driven mass of the payload is expected to play a major role. The relative mass of the Pb layer the purpose of which is to tamp outwards going hydrodynamic motion (besides radiation confinement) should also have some influence on η. Both effects have been investigated.

When changing the absorber parameters, we have decided to keep the payload mass (4 mg DT fuel and 20 mg PbLi pusher) as well as the payload radius $R_{PL} \cong 3$ mm constant. In a first series of implosions, the ion energy E_{ion} and the corresponding absorber thickness d have been varied. The calculated stopping lengths $d(E_{ion})$ with fractional energy loss in the Pb tamper fixed at 50 % are shown in Fig. 11. A beam pulse with uniform power and

$$P_{Beam} = I_{Beam} \cdot E_{ion} \qquad I_{Beam} = 50 \text{ kA}$$

$$E_{Beam} = P_{Beam} \cdot t_{pulse} \qquad t_{pulse} = 15 \text{ nsec}$$

has been used to implode the target. These parameters correspond to P_{Beam} = 500 TW and E_{Beam} = 7.5 MJ at E_{ion} = 10 GeV. The irradiation time has been chosen somewhat larger than optimal to insure mature implosion in all cases. Implosion runs have been performed with DT burn switched off and the results plotted in Fig. 12 are taken at the time of maximum fuel compression.

In the upper part of Fig. 12, it is seen that the hydrodynamic efficiency $\eta_{...}$ has a pronounced peak at $E_{...}$ = 3 GeV and falls rapidly when going

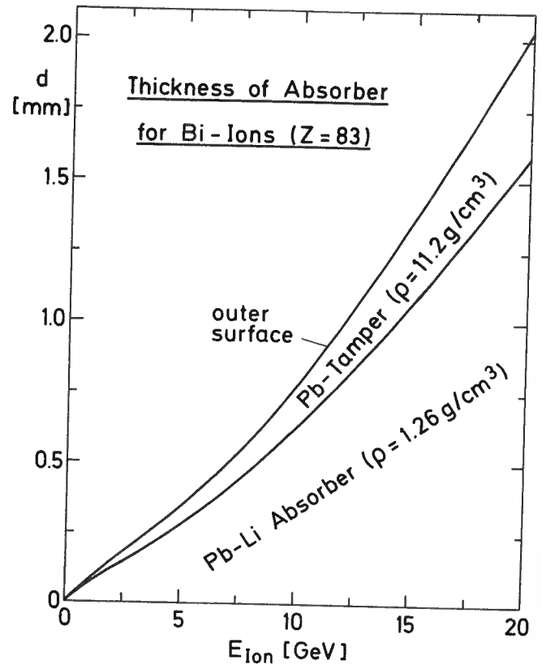

Fig. 11: calculated absorber thickness as a function of ion energy; 50 % energy loss occurs in the Pb tamper.

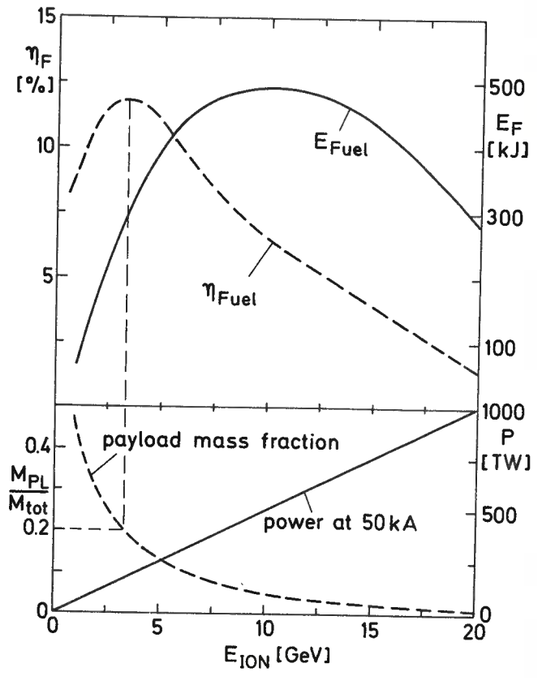

Fig. 12: Energy transfered to the fuel E_{Fuel} and hydrodynamic efficiency η_{Fuel} as a function of ion energy E_{ion} for fixed beam particle current of 50 kA with box pulse shape and for fixed payload (fuel and pusher) configuration of the target. In the lower part of the figure, the ratio of payload mass M_{PL} to total mass M_{tot} and the beam power are given.

to higher ion energies. The peak corresponds to 20 % payload mass fraction as shown in the lower part of Fig. 12. This is just the well known rocket optimum. Although the process of shell acceleration by ion beam deposition differs considerably from the rocket process of ablative acceleration, the overall momentum balance is similar and leads to the same optimum. This result is important because it allows for simple estimates. Maximum values of η_{Fuel} in optimized cases are around 15 %.

Instead of searching for maximum η_{Fuel} one may ask for the minimum beam current necessary to ignite the target. In view of the problems with beam transport this may be the more relevant question. For the 50 kA beam, the energy $E_{Fuel} = \eta_{Fuel} \cdot E_{Beam}$ is also plotted in Fig. 12. It peaks at E_{ion} = 10 GeV. We find in the present simulation that the maximum $E_{Fuel} \cong 500$ kJ is sufficient for ignition of the 4 mg fuel but not $E_{Fuel} \cong 300$ kJ obtained at E_{ion} = 3 GeV where η_{Fuel} has its maximum. In order to ignite the target using ions with $E_{ion} < 5$ GeV or $E_{ion} > 15$ GeV one would need a larger current. It is concluded that 10 GeV ions represent an optimum for this target.

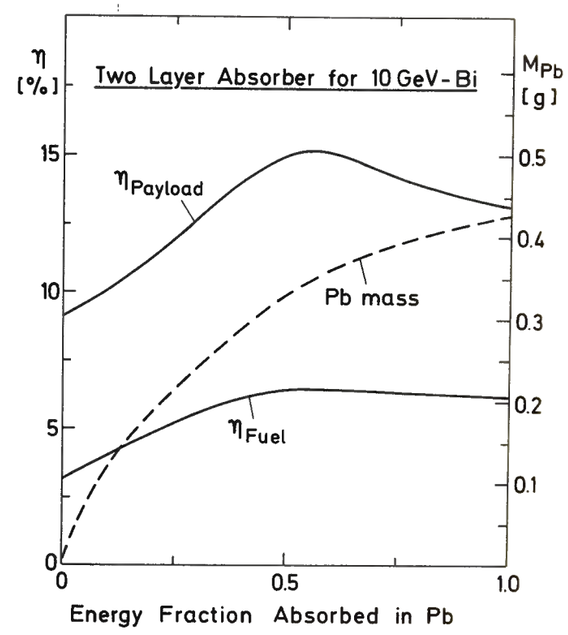

Fig. 13: Hydrodynamic efficiency of fuel η_{Fuel} and total payload $\eta_{payload}$ at time of void closure and the tamper mass as a function of beam energy loss in the tamper; beam (E_{ion}=10 GeV fixed) and payload configuration as given in Fig. 12.

In a second series of implosions, the masses of the absorbing layers have been varied under the constraint that they stop 10 GeV Bi ions. Results on the hydrodynamic efficiencies η_{Fuel} for the fuel and $\eta_{Payload}$ for the total payload at the time of void closure are given in Fig. 13 as a function of beam energy fraction absorbed in the tamper. For comparison, also the tamper mass is given. At void closure, $\eta_{Payload}$ is the relevant quantity representing the beam energy fraction which has been converted into kinetic energy of the supersonicly imploding target core. The increase of $\eta_{Payload}$ with increasing tamper mass is clearly seen. It rises almost a factor two and reaches an optimum for 50 % energy loss in the tamper.

4.3 The ignition problem

The gain model has shown that a fuel configuration at ignition consisting of a hot spark surrounded by cold compressed fuel is crucial for obtaining high gain. We have investigated the conditions under which such an ignition configuration is formed. The problem is to drive the innermost fuel part to much higher entropy than the outer fuel part. It may be solved either by a carefully timed superposition of shock waves or by a central ignitor. The underlying physics have been discussed in refs. 1 - 3. Here, we give examples for both concepts.

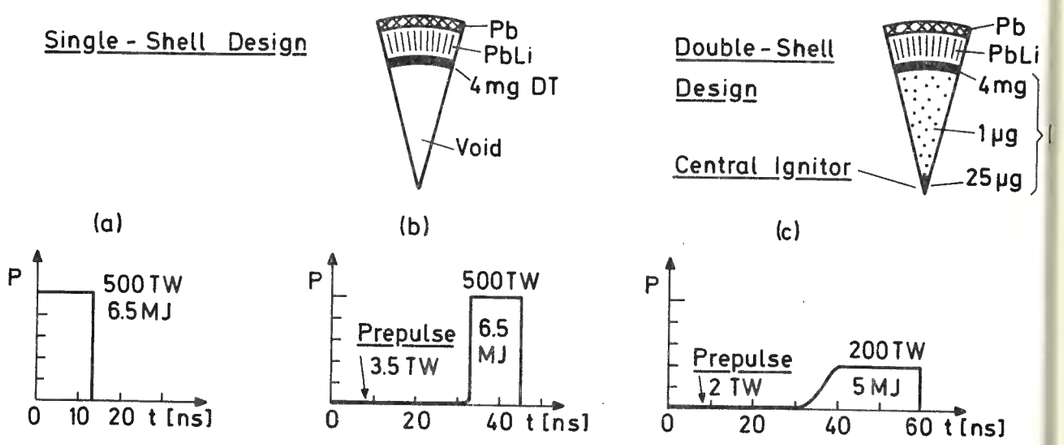

Fig. 14: Three different implosion cases: (a) single shell target with box pulse shape, (b) same as case (a) but with prepulse, (c) double shell target with central ignitor and a pulse shape including a prepulse.

Table 1 Implosion results for the cases defined in Fig. 14

	case (a) no prepulse	case (b) prepulse	case (c) central ignitor
pulse energy (MJ)	6.5	6.5	5
max. power (TW)	500	500	200
at ignition			
η_{Fuel} (%)	8.3	4.5	4.3
E_{Fuel} (kJ)	540	290	215
R_{Fuel} (µm)	230	127	160
$(\rho R)_{Fuel}$ (g/cm^3)	1.2	3.0	1.8
global parameters			
RT-efold Γ	6.0	12.3	8.6
impl. velocity (10^7cm/sec)	3.0	2.6	1.7
gain	144	170	210

Three different implosion cases are defined in Fig. 14 by giving the target configuration and the beam pulse. In all cases absorber, pusher and fuel layers are the same as in Fig. 8; in case (c) a solid DT sphere of 300 µm radius has been added as a central ignitor and 1 µg DT gas to fill the target cavity. Implosion results are given in Table 1. Within our present target simulation, all cases reach ignition (i.e. temperature larger than 5.6 keV in the center) with the specified values of pulse energy and maximum power. Dynamical details of case (a) and (b) are shown in Fig. 15. Enhanced entropy generation at the inner fuel surface during implosion requires at least two shock waves. In case (b), two strong shocks are produced by the onset of prepulse and main pulse leading to a well defined spark, whereas in case (a) a very strong first shock is created by the main pulse and a much weaker second shock occurs only indirectly due to fuel rarefaction and recompression. Case (a) is more impulsive; it leads to a rather smeared out entropy distribution over the fuel,

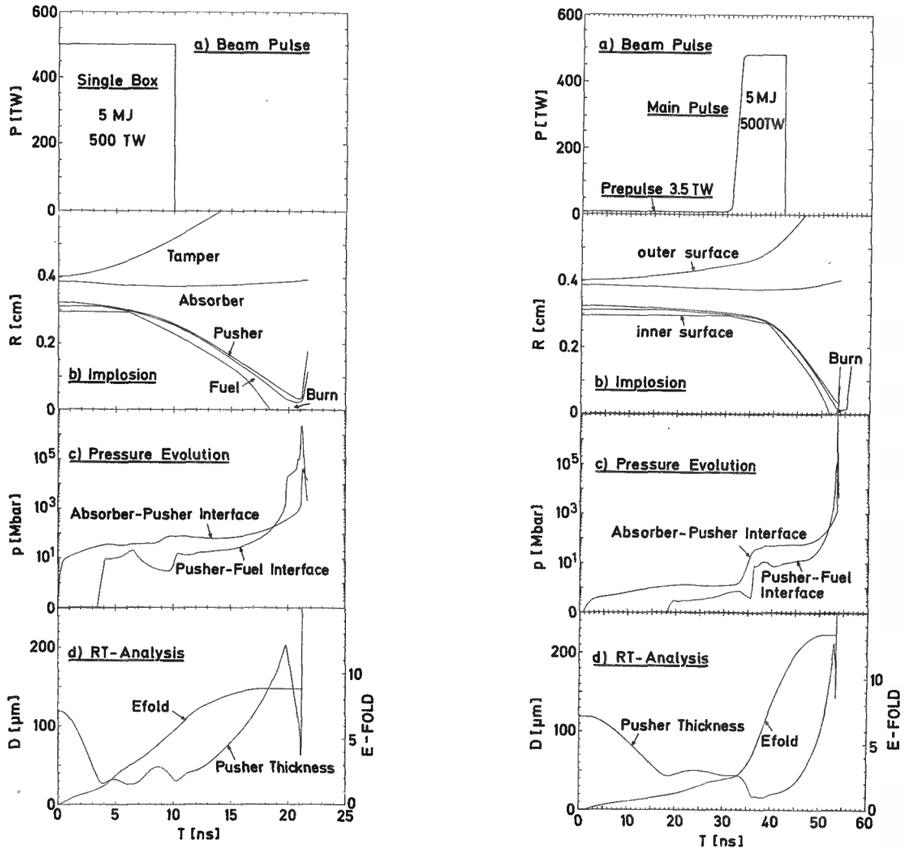

Fig. 15: Dynamical details of implosion without prepulse (case a, left side) and with prepulse (case b, right side).

but at the same time to a much higher η_{Fuel} and less sensitivity to Rayleigh-Taylor (RT) instability. The efold of RT-growth in the pusher has been estimated by

$$\Gamma = \int \sqrt{a(t)}/D(t)\, dt$$

where a(t) is the acceleration of the absorber/pusher interface and D(t) the pusher thickness. In case (c), the strength of the initial shocks is reduced by a smooth pulse shape and lower beam power. The spark region is produced when the rather isentropically imploding outer shell bumps into the central ignitor and causes strong shock heating.

The results given here should be considered as illustrations for different options to achieve ignition. We do not know how realistic they are. Certainly the effects of radiation transport which are not simulated so far have to be checked. Case (a) would be an attractive option due to its simplicity and relative stability. Case (c) has the advantage of low power requirements, but requires a rather complex target structure.

5. Selfsimilar compression waves

Intending to understand the basic physics of target implosion, we have studied selfsimilar spherical compression waves. We have reviewed published selfsimilar solutions relevant to inertial confinement fusion and have found a new one which describes non-isentropic collapsing hollow spheres and is therefore rather close to actual target implosions[11]. It follows from a direct generalisation of Guderley's work on imploding shock waves, but allows arbitrarily high compression.

A particularly interesting feature of this solution is that it describes the gas dynamics near the implosion center at times close to void closure including the reflected outgoing shock wave. This region is poorly described by numerical simulation based on difference methods, but is most important physically for ignition and burn. Here, we give

only some important conclusions which will hold approximately for target implosions in general:

1. uniform Mach number at time of void closure,
2. constant strength of the reflected shock which implies that this shock cannot be used for spark formation,
3. approximately uniform pressure behind the reflected shock which is the basic assumption of the gain model described above.

A particular solution of this selfsimilar type is shown in Fig. 16. For more details see ref. 11.

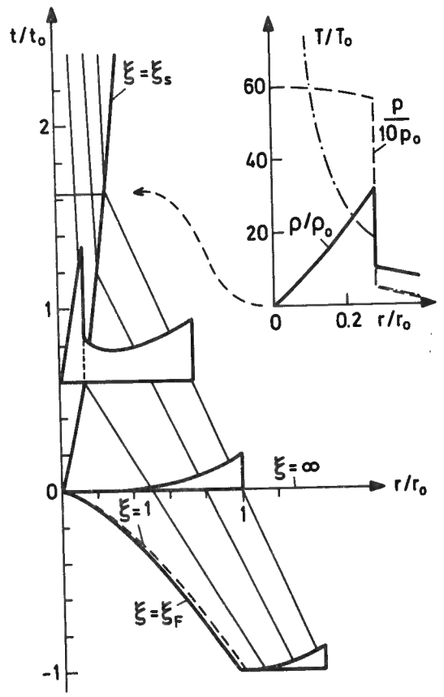

Fig. 16: Selfsimilar solution of an imploding, non-isentropic, hollow sphere in a (r,t) diagram. Trajectories of the imploding inner surface (ξ_F), the outgoing reflected shock (ξ_S) and some gas elements are seen. Density profiles at different times have been inserted; the separated insert also shows the distribution of pressure p and temperature T behind the reflected shock.

6. Foil Irradiation with Cylindrical Heavy Ion Beam. Scaling and Simulation.

For future experiments with intense heavy ion beams for inertial confinement fusion, scaling relations for the hydrodynamic response of irradiated target foils are derived and a simulation with a 2D PIC code is shown. A beam driven instability occurs which may cause problems in fusion targets.

A plane target foil is irradiated perpendicularly by a cylindrical heavy ion beam. Parameters are

beam intensity	ϕ
beam cross section	F
beam diameter	d
stopping length	λ ($\lambda \geq d$ assumed!)
target density	ρ
target atomic mass	μ
ion range	$R = \rho \cdot \lambda$
pulse length	Δt_{Pulse}

An illustration is given in Fig. 18. Uniform stopping power $dE/d(\rho x)$ is assumed. The energy deposited per unit mass of heated material (specific energy) then is

$$\varepsilon = (\phi \cdot F \cdot \Delta t_{Pulse})/(\rho \cdot \lambda)$$

The hydrodynamic response is given by the sound velocity $c \cong \sqrt{\varepsilon}$ of the heated material, and the response time is estimated as

$$\Delta t_{Target} \cong d/c = d/\sqrt{\varepsilon}$$

Maximum temperature, pressure etc. for target experiments are obtained when

$$\Delta t_{Pulse} \cong \Delta t_{Target}$$

Combining these equations, one obtains the basic scaling relation for maximum specific energy

$$\varepsilon_{Max} \cong (\phi \cdot d / \rho \cdot \lambda)^{2/3}$$

Ion Beam Irradiation of Al-Foil

(Ions e.g. 20 GeV Bi, 10 GeV Xe, 2 GeV Ar, 50 MeV α)

t = 0 ns

Ion Beam

$\Phi = 1\ TW/cm^2$

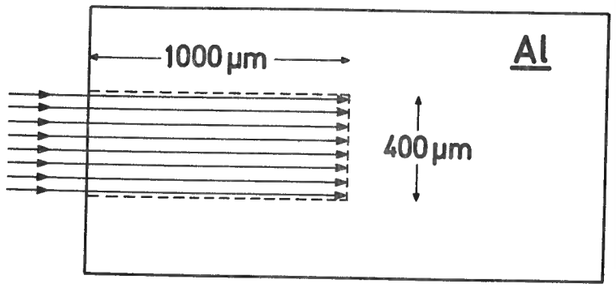

t = 18 ns

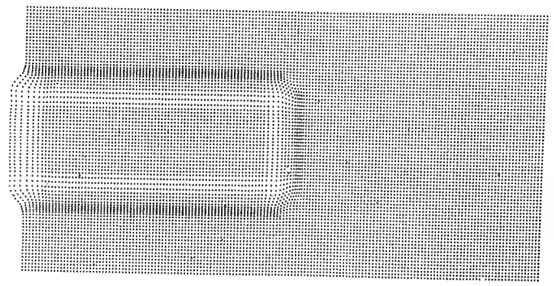

t = 34 ns

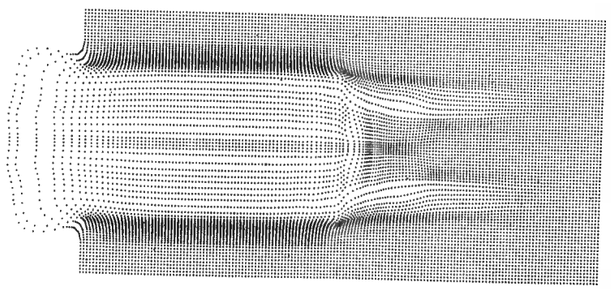

t = 58 ns

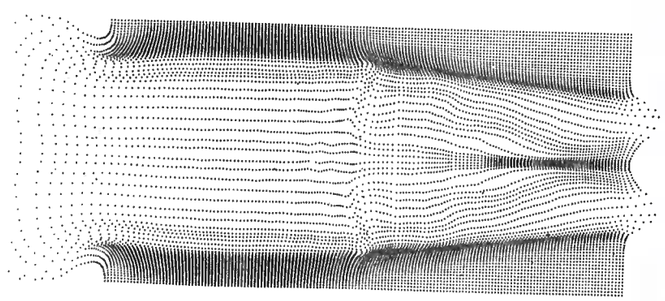

Fig. 18: Simulation with a 2D PIC code developed by Mulser

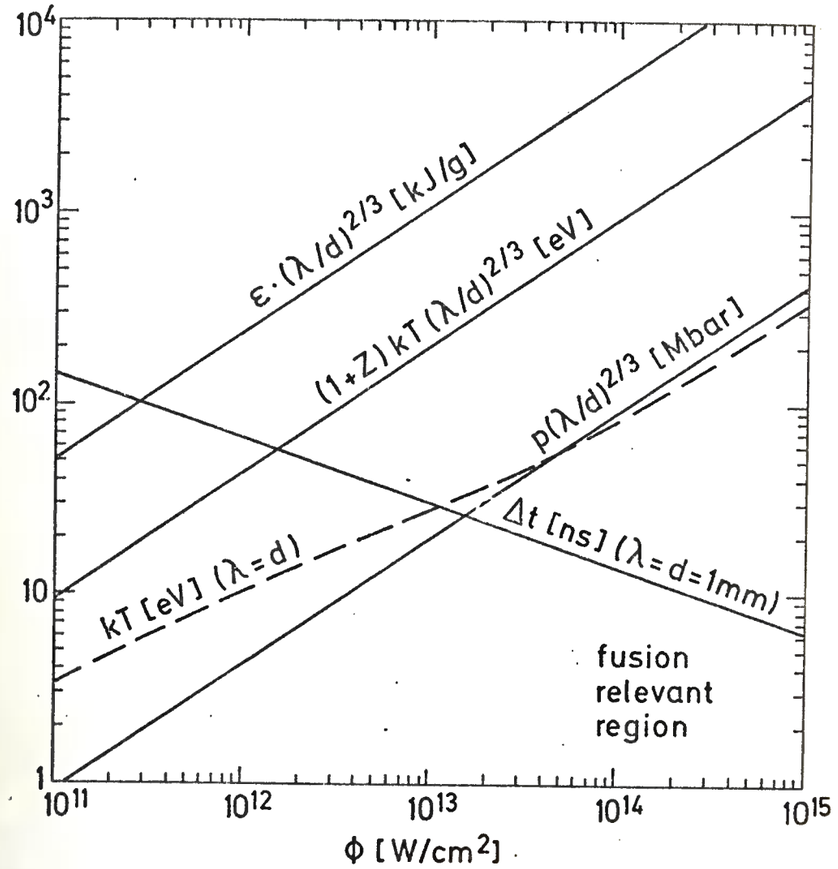

Fig. 17: Estimates for maximum specific energy ε, temperature T, pressure p and hydrodynamic response time Δt of a Al foil irradiated by an ion beam of intensity φ, diameter d and stopping length λ.

Maximum pressure and temperature follow from $p = 2\rho\varepsilon/3$ and $(1+Z(T))kT = 2\cdot\mu\varepsilon/3$ where Z(T) is the target ionization and an ideal gas equation of state is assumed. They scale like ε. The scaling of the response time is

$$\Delta t \cong (\phi/\rho\lambda)^{-1/3} \cdot d^{2/3}$$

The total pulse energy scales like

$$E_{Pulse} = \phi \cdot F \cdot \Delta t \cong \phi^{2/3} \cdot R^{1/3} \cdot d^{8/3}$$

These estimates are given in Fig. 17 for a Al foil ($\rho = 2.7\ g/cm^2$). A $\phi = 1\ TW/cm^2$ beam on a $1\ mm^2$ spot and $\lambda = d$ is estimated to produce a specific energy of 200 kJ/g, a pressure of 5 Mbar and a temperature of 10 eV after 50 nsec irradiation time.

A 2D simulation with a PIC code developed by P. Mulser[12] has been performed. Results for a $\phi = 1\ TW/cm^2$ beam with d = 0.04 cm, λ = 0.10 cm and Δt_{Pulse} = 100 nsec on a Al foil are shown in Fig. 18 in terms of density plots. At t = 18 nsec the center of the deposition region has been heated to 6 eV. Plasma is streaming out at the front surface, a shock wave is seen travelling outwards cylindrically and at the rear side and the beam heated material is rarefying at its surface. This rarefaction has the effect that the outer region of the cylindrical beam can now penetrate more deeply into the foil forming a hollow beam. The density distribution at t = 34 nsec and at t = 58 nsec in Fig. 1 shows that this hollow beam leads to cylindrical implosion as well as explosion at later time deeper in the foil and finally to a hole going through the 2 mm foil. This process of beam penetration beyond the initial stopping length is a beam driven instability which occurs due to non-uniform illumination. It may cause problems in fusion targets.

Conclusions

We have tried to present a qualitative picture of HIF target behaviour, to identify important parameters, to derive scaling relations and to give estimates. The presented model for target gain has shown that, independently of the type of driver, the gain depends predominantly on three free parameters:

the hydrodynamic efficiency	η_{Fuel}
the fuel isentrope	$\alpha_{Isentrope}$
the spark radius	r_{Spark}

The dependence on r_{Spark} is most dramatic, with ignition energy scaling

$$E_{ignition} \sim r_{Spark}^2$$

The spark radius is constrained by the degree of spherical symmetry during implosion

$$r_{Spark} \cong \xi \cdot r_{Focus}$$

where $\xi = r_{Spark}/r_{Fuel}$ is the lower limit of spherical convergence and directly driven targets are assumed with $r_{Fuel} \cong r_{Focus}$ and radii defined in Fig. 19. For the goal of heavy ion fusion to achieve high specific energy concentration ($\cong$ 600 MJ/g) for DT ignition, ξ and r_{Focus} are key parameters. For our estimates, it is assumed

$$\xi \cong 0.03$$

$$r_{Focus} \cong 3\ mm$$

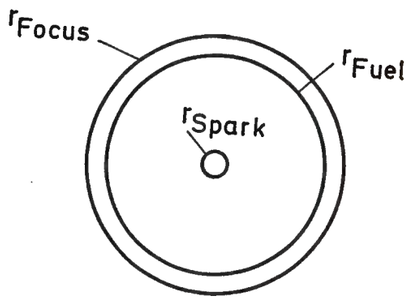

Fig. 19: Important radii for heavy ion driven targets

implying $r_{Spark} \cong 100\ \mu m$ and an energy of about 100 kJ in the hot central spark at ignition. Assuming η_{Fuel} = 10 %, this corresponds to a beam energy E_{Beam} = 1 MJ required for ignition. The scaling is $E_{Beam} \sim \eta_{Fuel} \cdot \xi^2 \cdot r_{Focus}^2$.

With respect to implosion dynamics, scaling relations for pulse time and beam power have been derived

$$\Delta t_{Pulse} \sim r_{Focus}/\sqrt{\varepsilon}$$

$$P_{Beam} \sim \varepsilon^{3/2} \cdot R(E_{ion}) \cdot r_{Focus}$$

with the specific energy deposition ε in the absorber and the ion range $R(E_{ion})$. Ranges for Bi ions on Pb and PbLi alloy have been

calculated. Target implosions driven by Bi-ions (HIBALL) have been studied numerically; they require typically $\Delta t_{pulse} \cong 10$ nsec, $P_{Beam} \cong 500$ TW and $E_{Beam} \cong 5$ MJ for a single shell reactor target with $E_{ion} = 10$ GeV, $r_{Focus} = 3$ mm and gain in the order of 100. Considerably less power (we find 200 TW) is needed for the same target when a central ignitor is used. The reason is that a much smaller implosion velocity is needed in this case to form the ignition spark.

The hydrodynamic efficiency η_{Fuel} of ion driven implosions of single-shell targets has been investigated, in particular, how it depends on the ion energy and the structure of the absorbing layers. A pronounced maximum of η_{Fuel} is found when the payload mass (fuel and pusher) amounts to 20 % of the total target mass. This is just the well known rocket optimum. For the HIBALL target, the optimum 10 % < η_{Fuel} < 15 % is obtained for $E_{ion} \cong 3$ GeV. In view of beam transport and focusing problems higher ion energies corresponding to lower beam currents may be preferable. Asking for the lowest beam current to ignite the HIBALL target, we find $I_{Beam} = 50$ kA with $E_{ion} = 10$ GeV, but now at a reduced hydrodynamic efficiency $\eta_{Fuel} \cong 5$ %. With respect to the absorber structure, a high-Z tamper around a low-Z absorber with higher stopping power is found to increase η_{Fuel}.

For future development of heavy ion fusion, it will be necessary to perform target experiments to test the physics of beam deposition as well as the hydrodynamic response. Ion range shortening with increasing temperature is predicted to set in appreciably around T = 100 eV. Our estimates show that such temperatures may be reached in Al foil targets at intensities of $\phi \cong 100$ TW/cm^2. Already with ion beams of 1 TW/cm^2 a very interesting state of matter with 100 000°K temperature and solid state density will be obtained which is difficult to be produced by other means. It may be used to study thermodynamic and radiative properties in this regime; also interesting hydrodynamic effects relevant for heavy ion fusion may occur such as the beam driven instability which has been discussed in this talk.

References

1. J. Meyer-ter-Vehn and N. Metzler, Target Design for Heavy Ion Beam Fusion, Max-Planck-Institut für Quantenoptik, Report MPQ 48, July 1981.

2. Untersuchungen zur Eignung von Schwerionenstrahlen für den Trägheitseinschluß, annual reports 1980 and 1981, published as GSI-Report.

3. HIBALL - A Conceptual Heavy Ion Beam Driven Fusion Reactor Study, Kernforschungszentrum Karlsruhe, Report KfK 3202, and University of Wisconsin, Report UWFDM-450, 1981.

4. R.E. Kidder, Laser Focus, Jan. 1982, pp. 65-66.

5. J. Meyer-ter-Vehn, Nucl. Fusion 22, 561, (1982).

6. R.E. Kidder, Nucl. Fusion 16, 405 (1976).

7. S. Bodner, Critical Elements of High Gain Laser Fusion, NRL Memorandum Report 4453, Jan. 1981.

8. J.H. Nuckolls, in LLL Laser Program Annual Report 1979, Vol. 2, p. 3-2.

9. see Y. Laichter et al., Proc. of this Symposium, 1982.

10. N. Metzler and J. Meyer-ter-Vehn, in preparation.

11. J. Meyer-ter-Vehn and C. Schalk, Selfsimilar Spherical Compression Waves in Gas Dynamics, to appear in Zeitschrift f. Naturforschung, Sept. 1982.

12. D. Lackner-Russo and P. Mulser, A Macroscopic PIC Code for Beam-Target Interaction Studies, Max-Planck-Inst. f. Quantenoptik, Report PLF 32, July 1980.